Supplement of Atmos. Chem. Phys., 21, 8293–8312, 2021
https://doi.org/10.5194/acp-21-8293-2021-supplement

Atmospheric Chemistry and Physics
Open Access

Supplement of

Carbonaceous aerosol composition in air masses influenced by large-scale biomass burning: a case study in northwestern Vietnam

Dac-Loc Nguyen et al.

Correspondence to: Hendryk Czech (hendryk.czech@uni-rostock.de)

Table S1. EC fractions, OC fractions and speciated organic compounds in $PM_{2.5}$ samples, including minimum (min.) and maximum (max.), as well as median, mean, 1st and 3rd quartiles (Q1 and Q3).

	Abbreviation	Unit	Min.	Q1	Median	Q3	Max.	Mean
Organic Carbon fraction	OC1	μg m^{-3}	0.00	0.00	0.12	0.42	1.05	0.23
Organic Carbon fraction	OC2	μg m^{-3}	0.38	0.64	1.21	1.87	7.07	1.73
Organic Carbon fraction	OC3	μg m^{-3}	1.21	2.38	4.11	6.94	15.30	5.23
Organic Carbon fraction	OC4	μg m^{-3}	0.21	0.74	1.58	3.05	7.96	2.25
Pyrolyzed Organic Carbon	OP	μg m^{-3}	0.00	0.03	0.76	2.89	8.29	1.85
Corrected Element Carbon	EC1-OP	μg m^{-3}	0.07	0.62	1.34	3.60	15.31	2.99
Elemental Carbon fraction	EC2	μg m^{-3}	0.06	0.48	1.22	2.05	3.09	1.25
Elemental Carbon fraction	EC3	μg m^{-3}	0.00	0.00	0.04	0.12	0.43	0.10
Organic Carbon	OC	μg m^{-3}	1.82	3.73	6.57	16.0	38.33	11.1
Elemental Carbon	EC	μg m^{-3}	0.13	0.83	2.05	2.98	9.80	2.41
Eicosanoic acid	A-C20	ng m^{-3}	0.03	0.04	0.08	0.23	0.66	0.17
Docosanoic acid	A-C21	ng m^{-3}	0.06	0.15	0.43	1.53	5.85	1.14
Tetracosanoic acid	A-C24	ng m^{-3}	0.05	0.23	0.76	3.00	12.46	2.25
Pentacosanoic acid	A-C25	ng m^{-3}	0.01	0.03	0.16	0.69	3.17	0.53
Hexacosanoic acid	A-C26	ng m^{-3}	0.03	0.12	0.62	2.30	11.38	1.86
Heptacosanoic acid	A-C27	ng m^{-3}	0.00	0.01	0.10	0.44	2.25	0.36
Octacosanoic acid	A-C28	ng m^{-3}	0.00	0.06	0.46	1.87	9.43	1.55
Nonacosanoic acid	A-C29	ng m^{-3}	0.00	0.02	0.04	0.37	1.85	0.30
Triacontanoic acid	A-C30	ng m^{-3}	0.00	0.02	0.26	1.34	6.58	1.10
Hentriacontanoic Acid	A-C31	ng m^{-3}	0.00	0.00	0.03	0.12	0.92	0.14
Dotriacontanoic Acid	A-C32	ng m^{-3}	0.00	0.00	0.13	0.67	3.16	0.52
Galactosan	GAL	ng m^{-3}	0.05	0.14	0.59	1.85	8.98	1.56
Mannosan	MAN	ng m^{-3}	0.68	1.45	5.28	18.6	60.2	12.9
Levoglucosan	LEV	ng m^{-3}	23.4	110	188	580	1710	437
Vanillin	VAH	ng m^{-3}	0.17	0.46	0.94	3.15	11.8	2.31
p-Hydroxybenzoic acid	p-H-acid	ng m^{-3}	0.31	2.12	7.60	43.0	192	34.1
m-hydroxybenzoic acid	m-H-acid	ng m^{-3}	0.35	1.48	4.66	16.6	45.3	10.5
Syringaldehyde	SYAH	ng m^{-3}	0.00	0.63	1.11	6.24	40.2	6.09
Syringic acid	SYA	ng m^{-3}	0.12	0.32	1.37	7.41	47.9	7.73
Vanillic acid	VA	ng m^{-3}	0.14	0.35	2.08	9.58	49.1	9.07
4-Nitrophenol	4-NP	ng m^{-3}	0.40	0.79	2.21	5.23	59.8	6.66
4-Nitrocatechol	4-NC	ng m^{-3}	0.20	0.45	2.32	5.19	616	41.5
2,6-Dimethoxy-4-nitrophenol	2,6-D-4-NP	ng m^{-3}	0.00	0.00	0.59	0.77	6.06	0.81
Eicosane	C20	ng m^{-3}	0.19	0.29	0.52	1.11	2.08	0.78

Heneicosane	C21	ng m^{-3}	0.60	0.85	1.57	2.93	4.69	1.94
Docosane	C22	ng m^{-3}	0.44	0.82	1.85	4.38	11.8	3.12
Tricosane	C23	ng m^{-3}	0.48	1.17	2.70	9.51	17.5	5.31
Tetracosane	C24	ng m^{-3}	0.78	2.05	4.02	7.39	16.1	5.84
Pentacosane	C25	ng m^{-3}	0.45	1.13	3.01	6.14	19.5	4.82
Hexacosane	C26	ng m^{-3}	0.54	1.40	2.29	4.64	16.9	4.02
Heptacosane	C27	ng m^{-3}	0.61	1.68	3.06	10.24	31.0	7.01
Octacosane	C28	ng m^{-3}	0.36	1.03	1.95	4.93	17.8	4.06
Nonacosane	C29	ng m^{-3}	0.53	1.49	4.55	18.46	58.8	12.7
Triacontane	C30	ng m^{-3}	0.54	0.92	1.73	4.21	11.5	3.10
Hentriacontane	C31	ng m^{-3}	0.49	1.09	4.59	16.69	43.4	10.4
Dotriacontane	C32	ng m^{-3}	0.17	0.36	0.82	1.89	6.27	1.48
Tritriacontane	C33	ng m^{-3}	0.22	0.44	1.63	4.95	14.4	3.47
Phenanthrene	PHE	ng m^{-3}	0.00	0.09	0.13	0.17	0.33	0.14
Fluoranthene	FLU	ng m^{-3}	0.01	0.03	0.03	0.05	0.09	0.04
Pyrene	PYR	ng m^{-3}	0.01	0.02	0.03	0.05	0.13	0.04
Benz[a]anthracene	BaA	ng m^{-3}	0.01	0.01	0.02	0.04	0.18	0.04
Chrysene	CHR	ng m^{-3}	0.02	0.03	0.03	0.06	0.17	0.05
∑Benzo[b,k]fluoranthene	BbkF	ng m^{-3}	0.04	0.10	0.16	0.28	0.67	0.23
Benz[e]pyrene	BeP	ng m^{-3}	0.03	0.09	0.16	0.25	0.42	0.19
Benz[a]pyrene	BaP	ng m^{-3}	0.00	0.01	0.02	0.03	0.13	0.03
Perylene	PER	ng m^{-3}	0.00	0.00	0.00	0.02	0.07	0.01
Indeno[1,2,3-cd]pyrene	IcdP	ng m^{-3}	0.02	0.02	0.04	0.05	0.09	0.04
Benzo[ghi]perylene	BghiP	ng m^{-3}	0.00	0.05	0.08	0.16	0.26	0.10
9H-Fluoren-9-one	9HFLUone	ng m^{-3}	0.29	0.48	0.59	0.76	2.24	0.75
1,8-Naphthalic anhydride	NAP-AN	ng m^{-3}	0.12	0.18	0.27	0.95	4.71	0.92
Naphthoic acid	NAP-AC	ng m^{-3}	0.12	0.32	0.77	1.21	9.13	1.62
9,10-Anthracenedione	9,10-AN	ng m^{-3}	0.29	0.48	0.59	0.76	2.24	0.75

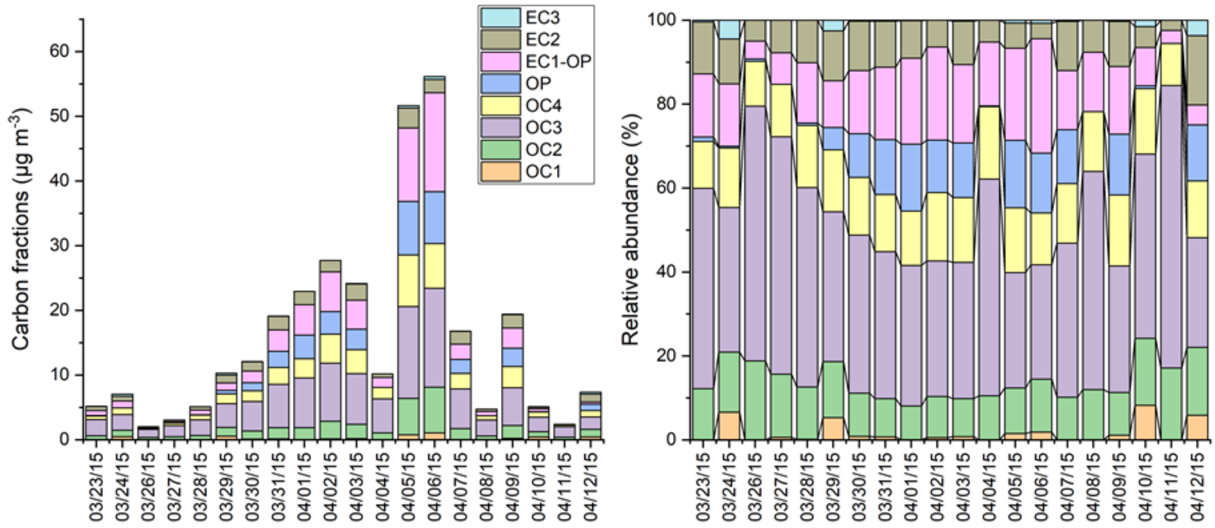

Figure S1. Time series of carbon fractions OC1, OC2, OC3, OC4, OP, EC1-OP, EC2 and EC3 in daily aerosol particle samples (n=20) at PDI during the sampling campaign from 23rd March to 12th April 2015 (see Table S1). Left column provides concentrations of each carbon fraction (µg m^{-3}), and right column provides relative mass fractions within carbonaceous fractions.

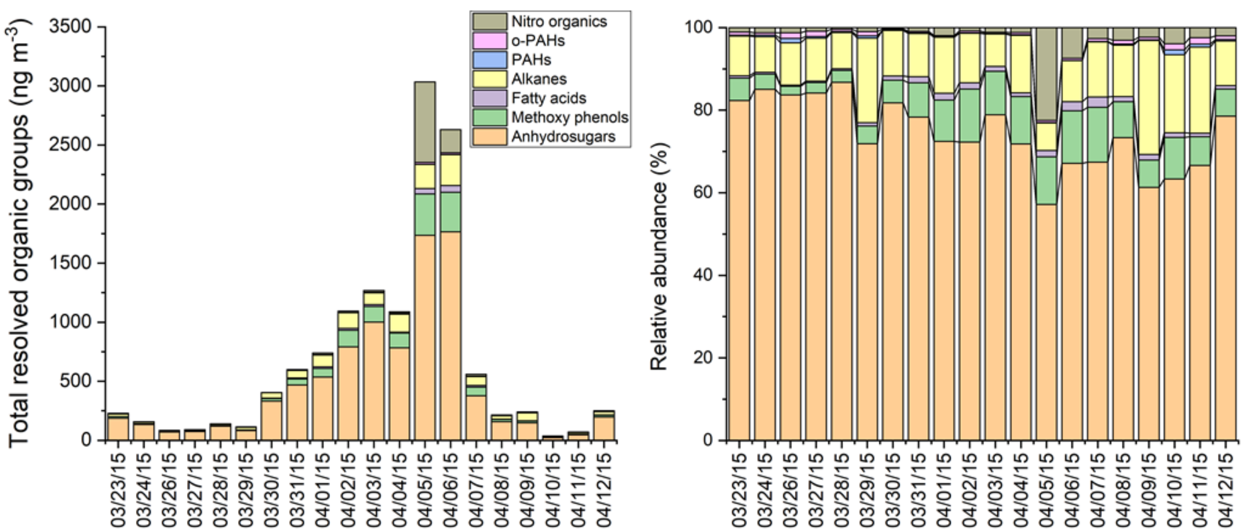

Figure S2. Time series of total resolved organic constituents in daily aerosol particle samples (n=20) at PDI during the sampling campaign from 23rd March to 12th April 2015. Left column provides identified mass concentrations (µg m^{-3}), and right column provides relative mass fractions within total class of compounds

Table S2 Concentrations of levoglucosan (LEV) and mannosan (MAN) from Bukowiecki et al. (2019) *Aerosol Air Qual. Res. 19*(5), 1172-1187, measured by high performance anion exchange chromatography with pulsed amperometric detection (HPAEC-PAD) from water-extracted quartz fiber filter samples.

Date in 2015	Levoglucosan	Mannosan	LEV/MAN
	[ng m^{-3}]	[ng m^{-3}]	[ ]
	ng m	ng m^{-3}	[ ]
March 22nd	475	68.9	6.89
March 23rd	79.3	85.9	0.92
March 24th	50.2	64.3	0.78
March 25th	n.a.	91.7	n.a.
March 26th	35.8	19.9	1.80
March 27th	48.99	16.8	2.92
March 28th	95.6	51.9	1.84
March 29th	81.8	26.1	3.13
March 30th	198	79.0	2.51
March 31st	487	51.6	9.42
April 1st	687	74.7	9.19
April 2nd	1104	60.3	18.32
April 3rd	1180	76.1	15.50
April 4th	915	88.6	10.33
April 5th	2280	137	16.69
April 6th	1890	104	18.10
April 7th	363	50.3	7.21
April 8th	109	40.4	2.71
April 9th	121	19.2	6.31
April 10th	2.44	26.5	0.09
April 11th	16.3	20.0	0.81
April 12th	119	16.0	7.47

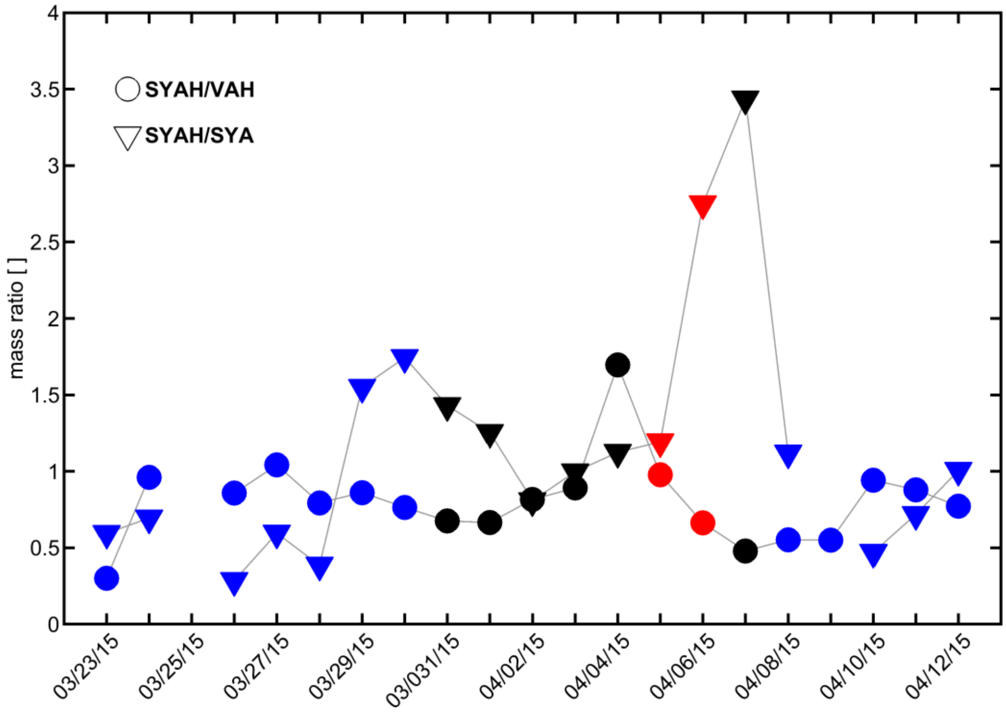

Figure S3. Mass ratios of syringic acid (SYAH) to vanillic acid (VAH, circles) and syringic acid (SYAH) to syringaldehyde (SYA, triangles). Colors correspond to days with low (blue), medium (black) and high BB-influence (red).

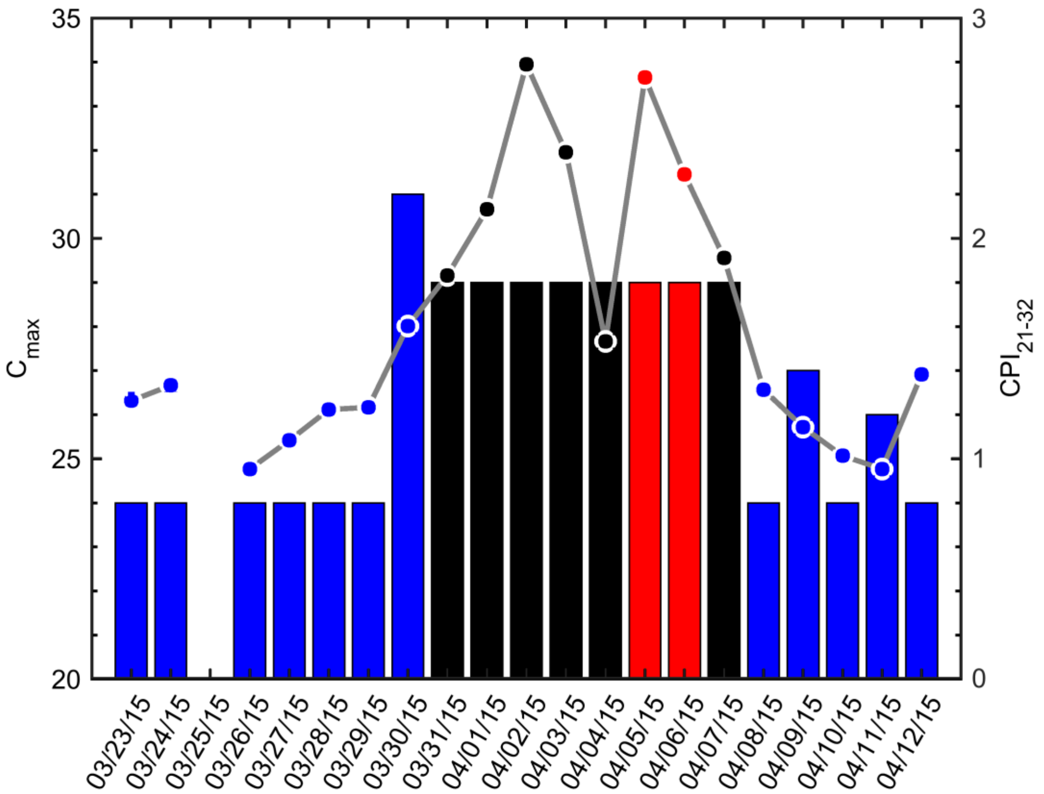

Figure S4. Carbon number of most abundant n-alkane (C_{max}; bars) and Carbon Preference Index (CPI) using n-alkanes from $C_{21}H_{44}$ to $C_{32}H_{66}$ (CPI_{21-32}; circles). Colors correspond to days with low (blue), medium (black) and high BB-influence (red).

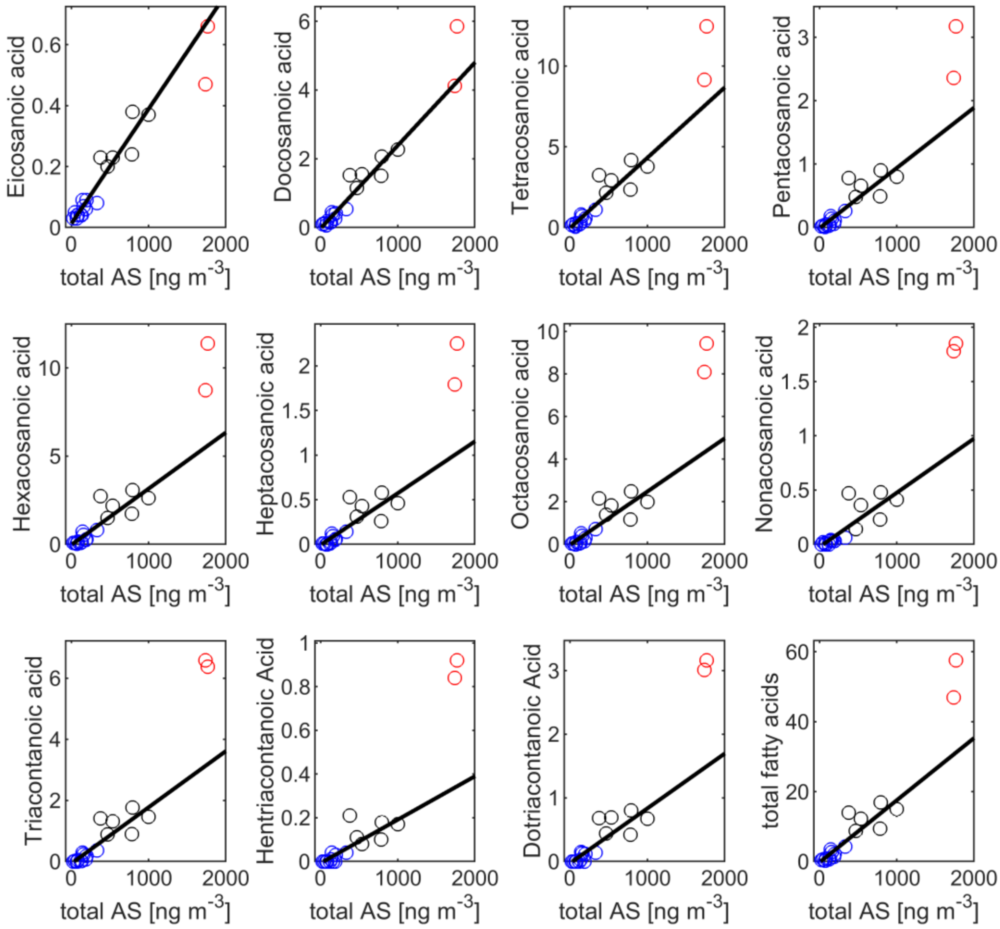

Figure S5. Illustration of concentrations of total anhydrosugars (AS) vs individual fatty acids and total fatty acids. Colors correspond to days with low (blue), medium (black) and high BB-influence (red). Linear regression functions (black lines) were obtained only from including days of low and medium BB-influence.

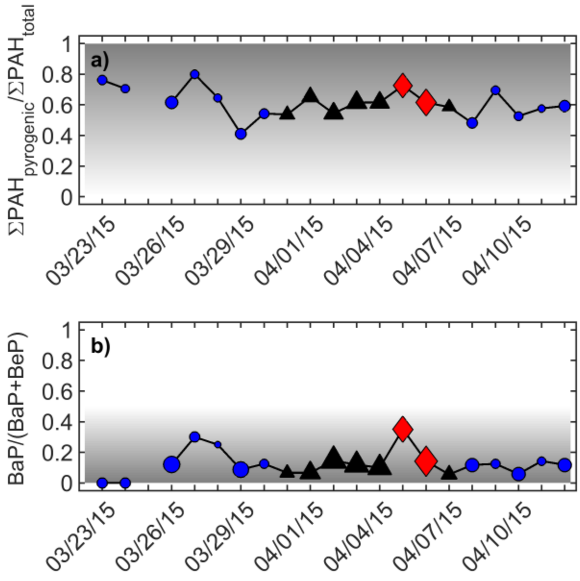

Figure S6. PAH diagnostic ratios to estimate **a)** the contribution of pyrogenic PAH and **b)** the influence of atmospheric aging. Colors denote the previously defined periods with low (blue), medium (black) and high (red) influence of BB. Dot sizes represent a relative metric for the total concentration of PAH involved in the respective diagnostic ratio. The gray-shaded area illustrates more PAH of pyrogenic origin and more atmospherically aged particles towards darker gray.

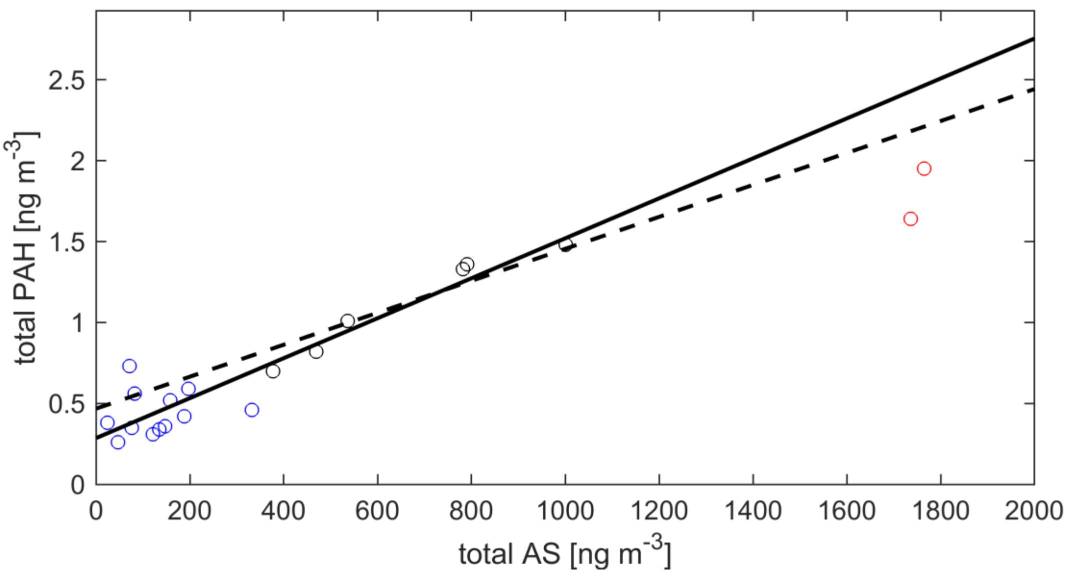

Figure S7. Illustration of concentrations of total anhydrosugars (A) vs total concentration 4- to 7-ring PAH. Colors correspond to days with low (blue), medium (black) and high BB-influence (red). Deming regression functions were obtained either only from including days of low and medium BB-influence (black solid line) or all data (black dashed line). Intercepts and slopes of the two fits are not significantly different at a significance level of 5%.

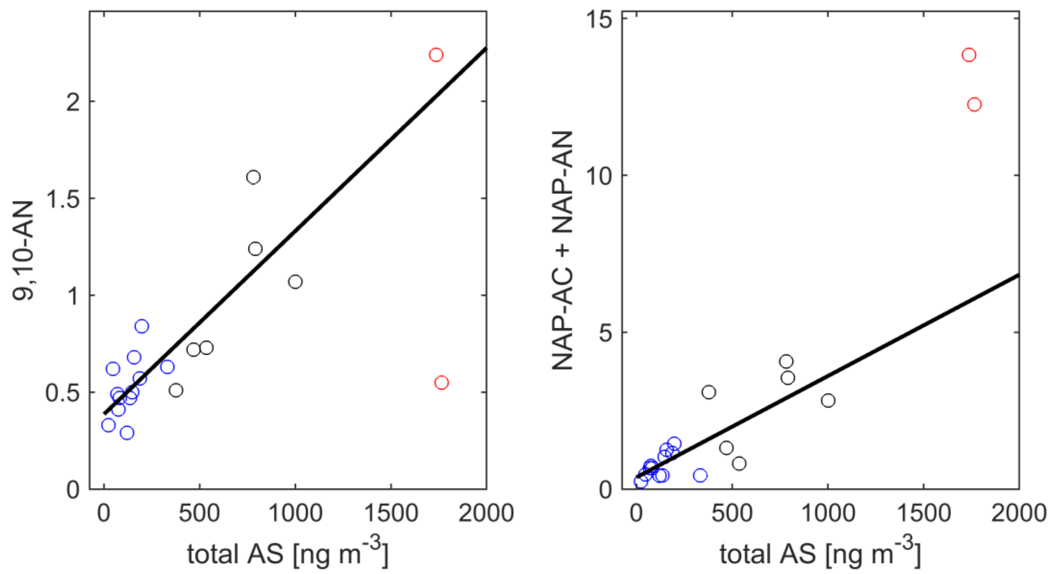

Figure S8. Illustration of concentrations of total anhydrosugars (AS) vs individual o-PAH 9,10-anthracenedione (9,10-AN) and the sum of naphthalic anhydride (NAP-AN) and naphthalic acid (NAP-AC). Colors correspond to days with low (blue), medium (black) and high BB-influence (red). Deming regression functions (black lines) were obtained by only including days of low and medium BB-influence (without days of high BB-influence).

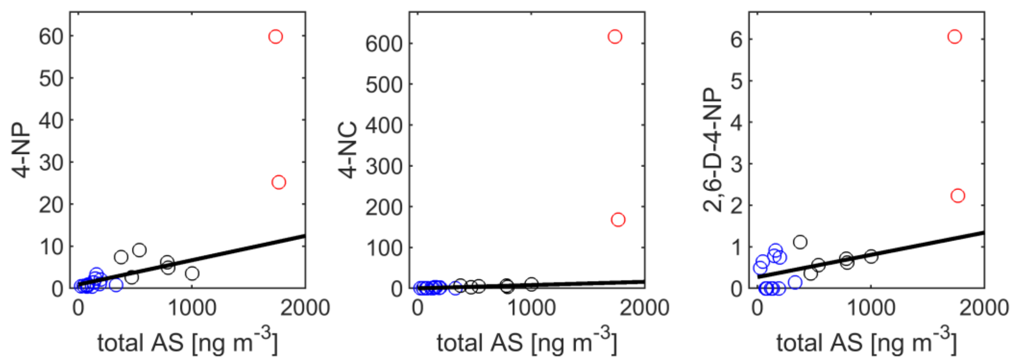

Figure S9. Illustration of concentrations of total anhydrosugars vs individual nitrophenols 4-nitrophenol (4-NP), 4-nitrocatechol (4-NC) and 2,6-dimethoxy-4-nitrophenol (2,6-D-4-NP). Colors correspond to days with low (blue), medium (black) and high BB-influence (red). Deming regression functions (black lines) were obtained by only including days of low and medium BB-influence (without days of high BB-influence).

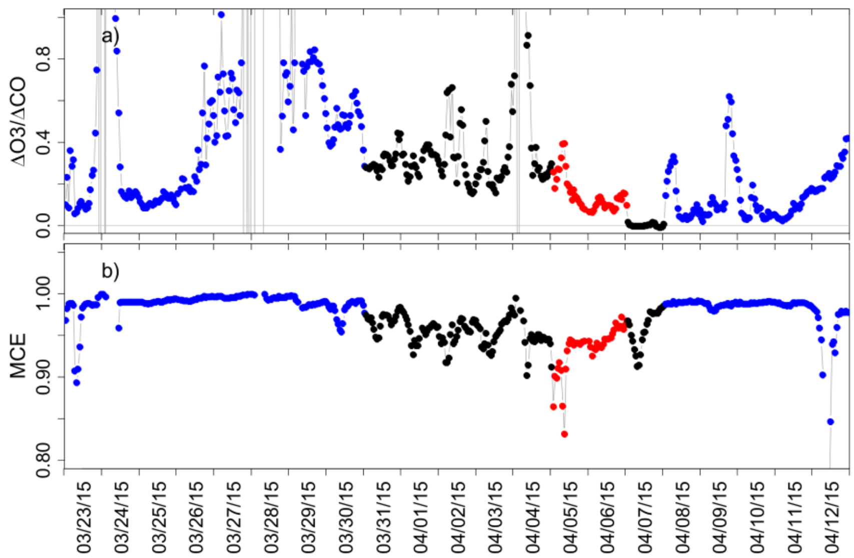

Figure S10. a) Hourly excess ratio between O_3 and CO ($\Delta O_3/(\Delta CO)$ ranged between 0.00 – 1.00. **b)** Hourly modified combustion efficiency (MCE: $\Delta CO_2/(\Delta CO+\Delta CO_2)$ ratios ranged between 0.80 – 1.00 at PDI during the sampling campaign from 23rd March to 12th April 2015. Colors denote the previously defined periods with low (blue), medium (black) and high (red) influence of BB.

Table S3. Fit coefficients for Deming regression of concentration = a·MCE+b (Figure 8) and their uncertainty by means of one standard deviation obtained from 500 Monte Carlo runs.

Compound class	Slope a [ng m^{-3}]	Intercept b [ng m^{-3}]
Anhydrosugars	-4.30e4 ± 1.39e4	4.25e4 ± 1.36e4
Fatty acids	-1.31e3 ± 420	1.30e3 ± 410
Methoxyphenols	-8.68e3 ± 2.70e3	8.58e3 ± 2.67e3
Nitrophenols	-1.48e4 ± 5.04e3	1.46e4 ± 4.89e3
n-alkanes	-5.90e3 ± 5.04e3	5.85e3 ± 4.89e3
PAHs	-41.8 ± 14.0	41.8 ± 13.7
o-PAHs	-337 ± 101	332 ± 99
OC	-844e3 ± 268e3	836e3 ± 263e3

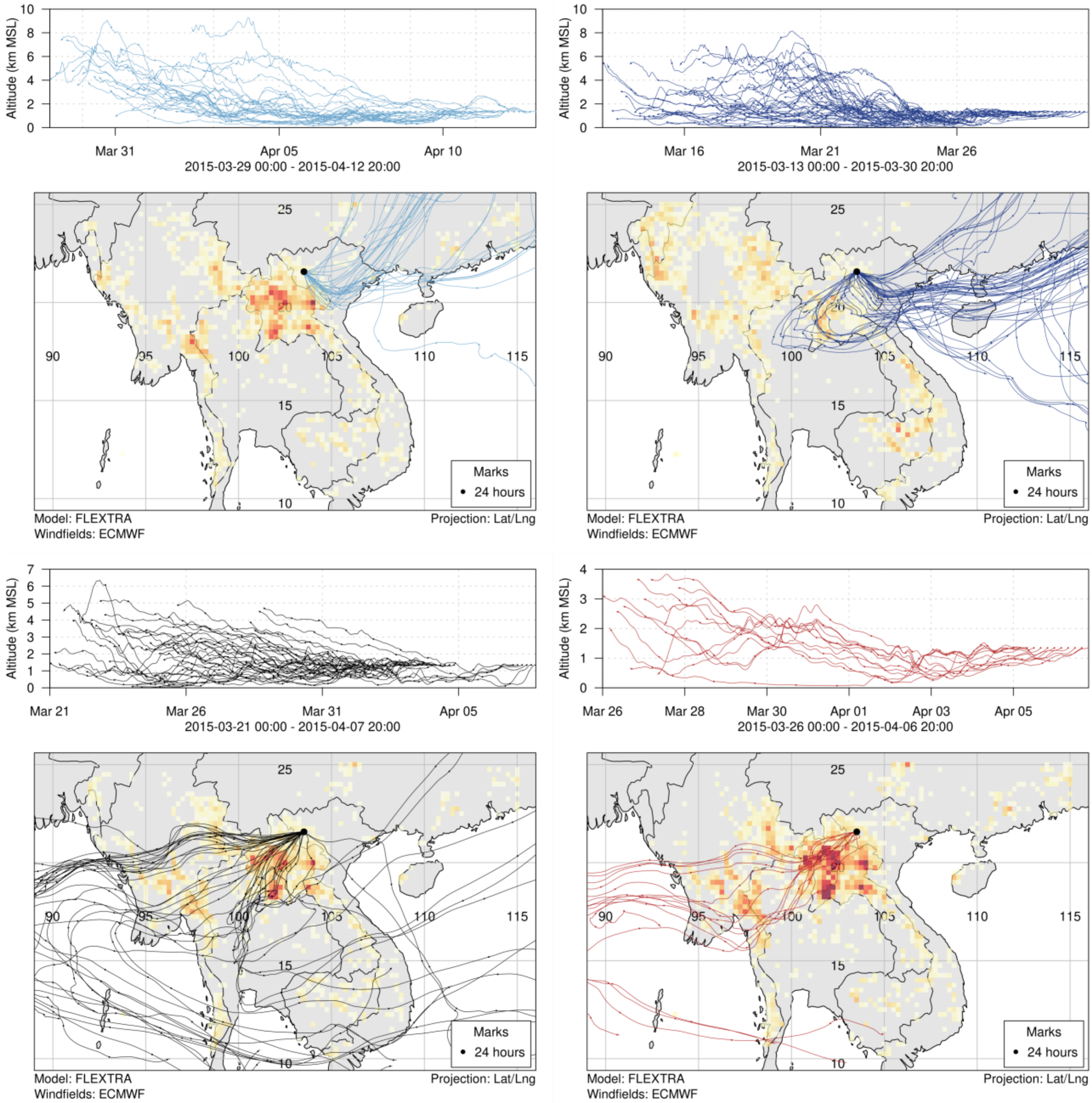

Figure S11. Ten-day backward trajectories arriving at PDI; the sub-periods were determined by the organic aerosol clustering 23 – 30 March (n=8, light blue), 31st March- 4th April + 7th April (n=6, black), 5th and 6th April (n=2, red), and 8th – 12th April (n=6, dark blue). The upper panels display the average height of the trajectories above sea level against time. The lower panel gives the average location of the trajectories overlaid on a map of MODIS fire count densities for the period five days before the beginning of each sub-period until the end of each sub-period (from low (bright yellow) to high (orange-red) fire intensities).